Research Square

Preprints are preliminary reports that have not undergone peer review.
They should not be considered conclusive, used to inform clinical practice,
or referenced by the media as validated information.

On-site solar PV and storage make European truck charging stations more affordable and grid-friendly under heterogeneous network tariffs

Kun Gao

gkun@chalmers.se

Chalmers University of Technology https://orcid.org/0000-0002-4175-850X

Xiaohan Liu

Chalmers University of Technology

Patrick Plötz

Fraunhofer Institute for Systems and Innovation Research ISI https://orcid.org/0000-0001-6790-0183

Sonia Yeh

Chalmers University of Technology https://orcid.org/0000-0002-4852-1177

Xiaobo Qu

Tsinghua University https://orcid.org/0000-0003-0973-3756

Article

Keywords:

Posted Date: September 29th, 2026

DOI: https://doi.org/10.21203/rs.3.rs-10581612/v1

License: This work is licensed under a Creative Commons Attribution 4.0 International License.
Read Full License

Additional Declarations: There is **NO** Competing Interest.

On-site solar PV and storage make European truck charging stations more affordable and grid-friendly under heterogeneous network tariffs

Xiaohan Liu[1], Patrick Plötz[2,3], Sonia Yeh[3], Xiaobo Qu[4*], Kun Gao[1*]

[1]Department of Architecture and Civil Engineering, Chalmers University of Technology, Chalmersplatsen 1, Göteborg, 41296, Sweden.
[2]Fraunhofer Institute for Systems and Innovation Research ISI, Breslauer Straße 48, Karlsruhe, 76139, Germany.
[3]Department of Environmental and Energy Sciences, Chalmers University of Technology, Chalmersplatsen 1, Göteborg, 41296, Sweden.
[4]School of Vehicle and Mobility, Tsinghua University, Haidian District, Beijing, 100084, China.

*Corresponding author(s). E-mail(s): gkun@chalmers.se; xiaobo@tsinghua.edu.cn;
Contributing authors: xiaohanl@chalmers.se; patrick.ploetz@isi.fraunhofer.de; sonia.yeh@chalmers.se;

Abstract

Megawatt charging is central to long-haul truck electrification, but deployment is constrained by long grid-connection lead times and exposure to heterogeneous, evolving network tariffs. Using time- and space-resolved charging demand for 2,310 optimised charging locations across Europe and real tariff schedules from 160 European distribution system operators, we identify network-tariff heterogeneity as a previously underappreciated determinant of charging-infrastructure economics. Network tariffs alone create levelised charging-cost (LCOC) spreads of 0.03–0.04 EUR kWh^{-1} between best- and worst-case tariff designs, comparable to the infrastructure cost of charging itself. On-site solar PV with energy storage can halve these tariff-driven LCOC differences, cut LCOC by at least 20% for 42% of locations, and postpone the point at which median net peak power reaches half of grid-connection capacity by up to five years. By quantifying how local flexibility compresses tariff-driven cost differences and grid constraints,

our analysis provides a broader framework for integrating emerging large electricity loads into constrained distribution networks, showing how long-haul truck charging hubs can shift from passive, tariff-exposed loads into controllable and grid-friendly assets.

Heavy-duty vehicles make up less than 8% of the on-road fleet but emit over 35% of road transport CO_2 [1]. Long-haul freight is among the hardest transport segments to decarbonise [2]. High-power charging (megawatt charging systems (MCS) and combined charging systems (CCS)) is central to this transition, letting electric trucks recharge during statutory rest periods without disrupting logistics operations [3]. However, by enabling high-power en-route charging, MCS shifts challenges from vehicle range and charging time to infrastructure deployment, including high-capacity grid connections, local peak demand, and network-tariff exposure, which determine the economic feasibility and grid impacts of deploying charging infrastructure [4–6].

A major hurdle is the availability and timing of high-power grid connections. Securing megawatt-scale grid connections for MCS involves long lead times, grid reinforcement, and uncertain approval processes [7–9]. These slow infrastructure rollout and expose charging point operators (CPOs) to investment risk. Compounding this, European network tariffs are rising and fragmenting. Electricity costs may double by 2050 [10], amid roughly 2,400 distribution system operators (DSOs) across Europe [11], including 883 in Germany alone in 2019 and several countries above 100 [12]. Many are shifting to power-based and time-of-use tariffs [13], which can dominate operating costs at high-power charging stations where demand concentrates in narrow time windows. Substantial heterogeneity in tariff designs among regions [14] further compounds uncertainty in levelised cost of charging (LCOC) for deploying MCS. The high and uncertain costs are likely be passed on to users, raising societal charging costs and slowing logistics electrification.

Existing studies have advanced understanding of electric trucks and charging costs [15–17], but critical gaps remain. Most analyses fail to resolve charging demand jointly in time and space at the station level across the full EU network, leading to misrepresented peak loads, underestimated exposure to power-based tariffs, and biased estimates of LCOC and grid impacts. Some studies derive time-varying demand only in aggregate [18], while others assign node-level demand without capturing its temporal variation [19]. Station-level economic studies have instead focused on depot charging using CCS, where demand is predictable and grid impacts limited [7, 20] or covered only narrow spatial extents. This is a critical omission for MCS. Unlike depot charging, en-route charging demand is opportunistic, uncoordinated, uneven across locations, and highly time-dependent [21], directly shaping peak loads, grid-connection requirements, and LCOC. Ignoring these dynamics risks suboptimal charger siting and may worsen existing grid constraints including grid-connection delays. On-site solar photovoltaic (PV) and energy storage offer a potential remedy by reducing net grid demand and smoothing peak loads [22, 23]. However, their value depends on interactions with

time-varying charging demand and local tariffs. It remains unresolved whether PV and energy storage can make truck charging stations economically feasible, hedge power-based tariff exposure and mitigate grid-capacity scarcity across the European network.

This research shows that high-power truck charging stations can be transformed into economical and grid-friendly facilities whose economics and grid impacts are substantially reshaped by on-site PV and storage. We make two major contributions. First, we derive optimised charging infrastructure deployment (siting and sizing) and LCOC for charging stations across EU countries and tariff structures, grounded in hour-resolved and node-level charging demand from EU continent-scale long-haul freight flow. Second, we quantify how on-site solar PV and energy storage reduce LCOC, reshape tariff exposure, and preserve grid-connection headroom, with meaningful implications for investment economics, charging affordability, and the long-term scalability of charging rollout for electric EU freight.

Network-tariff heterogeneity creates large LCOC difference of truck charging stations

Meeting projected 2034 en-route charging demand of the European logistics network requires 2,310 charging locations across 36 European countries (Fig. 1), comprising 13,569 100-kW CCS chargers for long rests and 7,304 1-MW MCS chargers for short breaks. Requirements are spatially heterogeneous, mirroring the uneven distribution of European freight flows (Figs. 1a and b). Germany, France, Spain and Italy dominate, requiring 329, 277, 162, and 161 locations with 4,275, 4,578, 1,496, and 1,003 chargers, respectively, while several countries need fewer than 10 locations (Supplementary Table 1). Heterogeneity persists at the station level (Fig. 1c): 60% of locations, mostly along peripheral routes, need five chargers or fewer, while 10%, mostly in high-traffic corridors across Germany and France, require 21 or more. Country-level results are summarised in Supplementary Table 1.

LCOC at each location is the sum of infrastructure overhead and electricity costs, the latter computed from country-level average electricity prices. Country-level medians of LCOC, lifetime served demand, and electricity price are mapped in Fig. 2a–c. LCOC is primarily co-determined by served demand and electricity price: high utilisation and low prices compress LCOC, and vice versa. Sweden (0.15 EUR kWh^{-1}), Portugal (0.17 EUR kWh^{-1}), Denmark (0.20 EUR kWh^{-1}), and Spain (0.21 EUR kWh^{-1}) achieve the lowest median LCOC (Fig. 2d), reflecting high utilisation and low electricity prices. Hungary (0.32 EUR kWh^{-1}), the Netherlands (0.33 EUR kWh^{-1}), and the United Kingdom (0.39 EUR kWh^{-1}) exhibit 2.1, 2.2, and 2.6 times the Swedish benchmark, driven by lower utilisation and higher electricity prices. Within-country dispersion is pronounced (Fig. 2d), driven by site-level demand variation, with Finland, Moldova, North Macedonia, and Ukraine showing the largest variation. Substantial station-level spatial heterogeneity is further illustrated in Fig. 2e. These results expose deep inequities in CPO investment economics and disparities in end-user charging costs across Europe, with direct consequences for the pace and affordability of freight electrification under competitive markets.

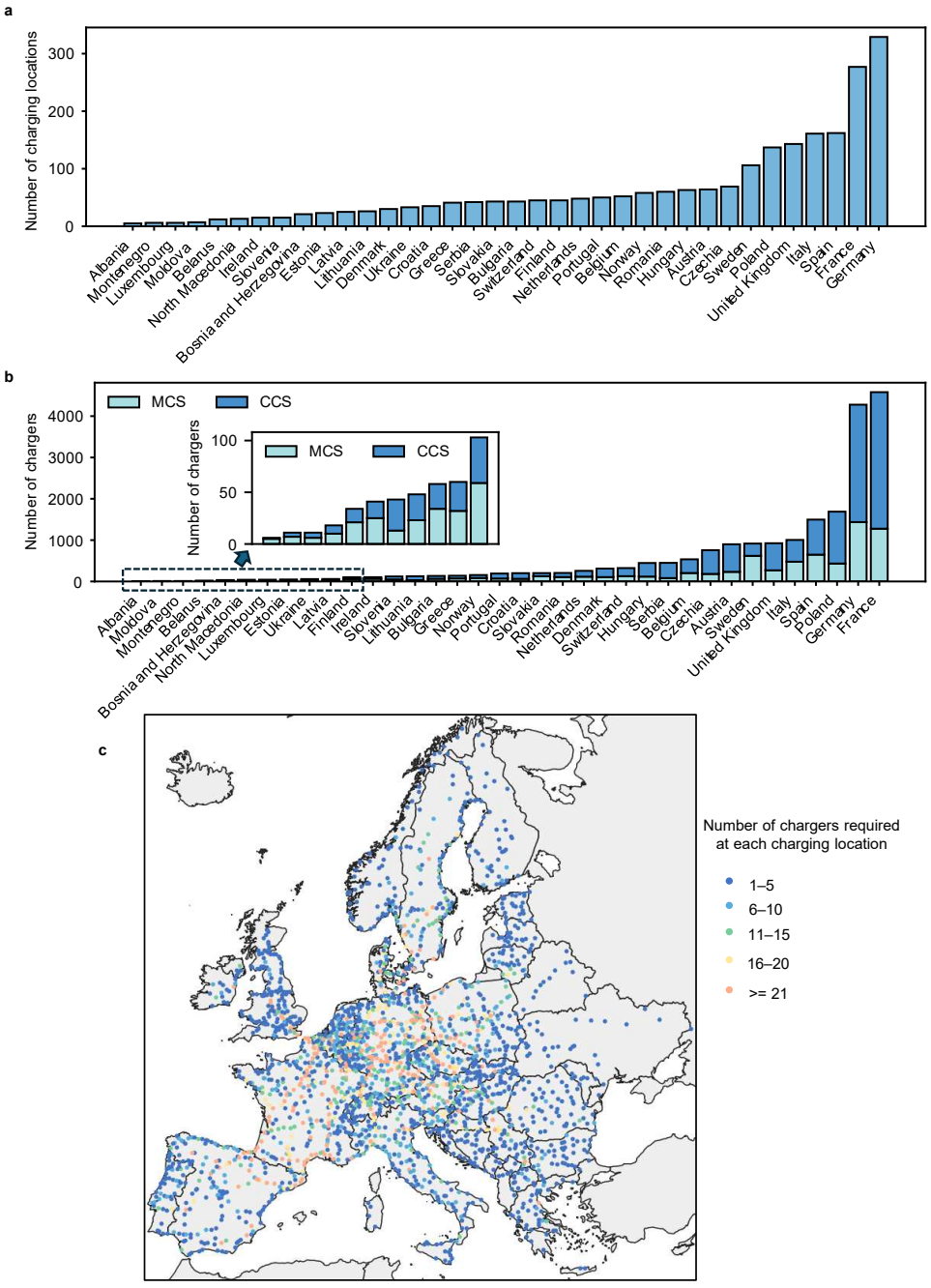

Fig. 1 a-c, Optimised charging infrastructure for en-route charging across the European network. (a), Number of charging locations required at the country level. (b), Number of CCS and MCS chargers required at the country level. (c), Charging locations and the number of chargers required at each charging station.

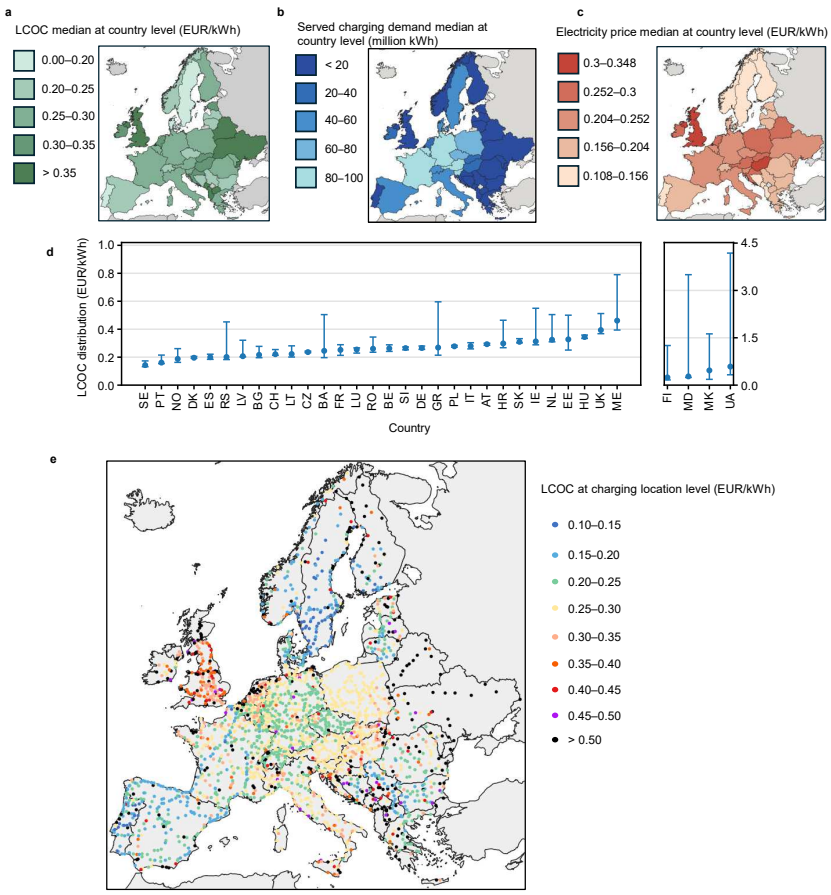

Fig. 2 **a**–**c**, Country-level medians of (a) LCOC, (b) lifetime served charging demand and (c) electricity prices derived from Eurostat [24] and the UK statistical data [25]. **d**, Distribution of LCOC values (median with the 25th–75th percentile range) at the charging location level within each country (excluding Albania and Belarus). **e**, Spatial distribution of LCOC across charging locations in Europe.

To investigate network-tariff effects on station-level LCOC, we construct two tariff scenario pools: Pool-SE (115 Swedish DSO tariffs; Supplementary Figs. 1, 2) and Pool-DE (45 German DSO tariffs; Supplementary Figs. 3, 4). For each location, we evaluate LCOC under all tariff schemes in each pool and identify the highest and lowest LCOC as "worst" and "best" cases. The median worst-to-best LCOC difference ($\Delta LCOC$) (Fig. 3a) reaches 0.04 and 0.03 EUR kWh^{-1} for Pool-SE and Pool-DE, respectively, matching or exceeding the median infrastructure cost component of LCOC (0.03 EUR kWh^{-1}). At 70% of locations in Pool-SE and 55% in Pool-DE, the tariff-driven $\Delta LCOC$ exceeds the infrastructure cost component. In relative terms (i.e., $\Delta LCOC$ normalised by the best-case LCOC), the median tariff-driven $\Delta LCOC$ (Fig. 3b) is 15.7% in Pool-SE with nearly 30% of locations exceeding 20%, and is

11.4% in Pool-DE with 7% locations exceeding 20%. Country-level distributions of the relative worst-to-best LCOC differences for Pool-SE and Pool-DE are presented in Supplementary Figs. 5 and 6, respectively, showing that countries with lower baseline LCOC tend to be more sensitive to network-tariff heterogeneity.

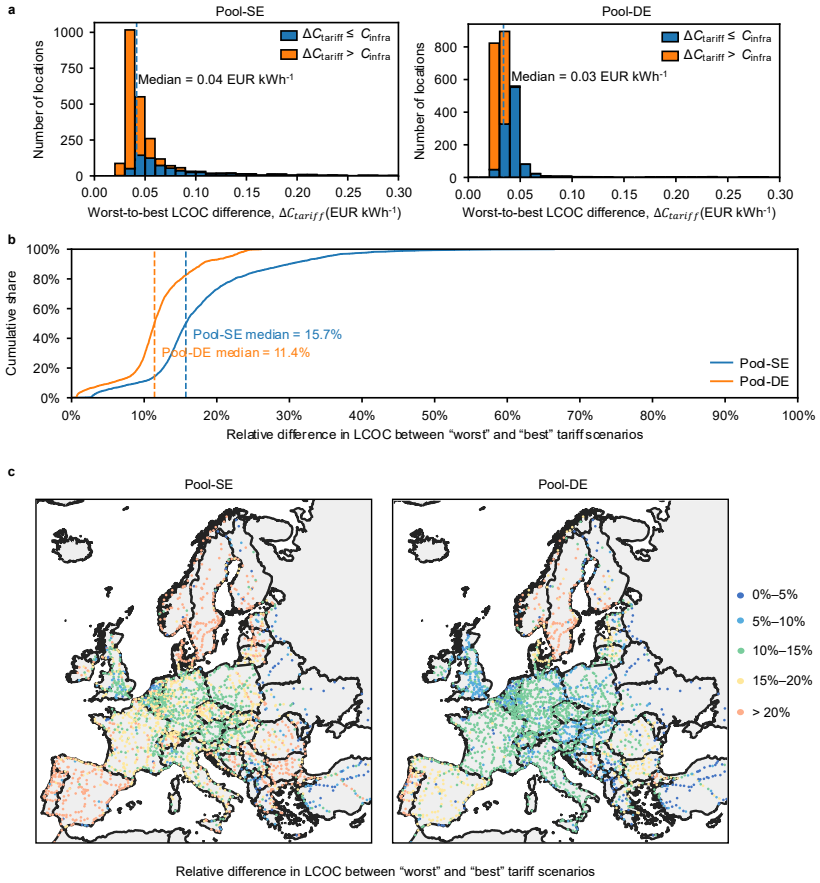

Fig. 3 **a**, Distributions of the absolute worst-to-best LCOC difference, ΔC_{tariff}, under Pool-SE and Pool-DE. Bars are stacked according to whether the tariff-driven $\Delta LCOC$ is smaller than or equal to, or larger than, the infrastructure component of LCOC, C_{infra}. The x-axis is truncated at the 99.5^{th} percentile of ΔC_{tariff} to improve readability. **b**, Cumulative distributions of the relative differences in LCOC between "worst" and "best" tariff scenarios across charging locations in Pool-SE and Pool-DE, respectively. **c**, Spatial distributions of the relative differences in LCOC between "worst" and "best" tariff scenarios across charging locations in Pool-SE and Pool-DE, respectively.

These findings indicate that network-tariff exposure can rival the infrastructure cost itself in reshaping LCOC, with direct consequences for end-user charging costs. Minor differences between the Pool-SE and Pool-DE tariff structures (discussed in Supplementary Note 1) do not alter the main conclusions. A central 90% tariff-driven difference (P95–P5) confirms this is not driven solely by extreme tariffs, remaining

close to the infrastructure cost component at 0.028 and 0.026 EUR kWh^{-1} for Pool-SE and Pool-DE, respectively.

Fig. 3c summarises relative tariff-driven $\Delta LCOC$ at each station, revealing substantial spatial variation. Decomposing network costs into energy- and power-charge components (Supplementary Fig. 7) shows that, under worst-case tariffs, Pool-SE's median energy- and power-charge components rise to roughly five and fifteen times their best-case values, respectively, while Pool-DE's roughly double. These results show that network-tariff design alone can substantially alter station-level LCOC through large differences in both energy- and power-related charges, making tariff structure a key determinant of charging-station economics, and under competitive markets, this effect ultimately passes through to end-user charging costs.

On-site solar PV and energy storage reshape LCOC of charging locations

We assess how on-site solar PV and energy storage reduce LCOC across three PV-siting scenarios (conservative, moderate, and optimistic) and three storage scenarios (none; 373 EUR kWh^{-1}, the EU-projected cost; 100 EUR kWh^{-1}, an optimistic future cost). For PV-siting scenarios, the conservative scenario restricts deployment to existing rooftop and ground areas at truck-parking sites identified from Google Maps. The moderate and optimistic scenarios cap the feasible deployment area at 5,000 m^2 and 10,000m^2, respectively, unless the conservative mapped area is larger. The baseline excludes on-site PV or storage. all deployments are sited and sized according to station-level demand and the tariffs in Pool-SE and Pool-DE (see Methods).

Station-level LCOC reductions are summarised in Fig. 4a (Pool-SE) and b (Pool-DE). Under Pool-SE, PV alone yields median LCOC reductions of 2%, 7%, and 11.9% under conservative, moderate, and optimistic PV-siting scenarios, respectively. Storage adds only marginally to the median LCOC reduction (2.1%, 7.8%, 12.7% at 373 EUR kWh^{-1} cost; 2.8%, 10%, 15.9% at 100 EUR kWh^{-1} cost), but its distributional effect is more consequential. With energy storage, the share of stations achieving LCOC reductions of $\geq$12%, $\geq$16%, and $\geq$20% increases substantially relative to PV alone, particularly under moderate and optimistic scenarios. For example, under the moderate scenario, the share achieving $\geq$12% and $\geq$16% reductions rises from 30% and 17% under PV alone to 44% and 33% with 100 EUR kWh^{-1} storage; under the optimistic scenario, PV with low-cost storage pushes 60% and 42% of stations past 12% and 20% reductions, respectively. Pool-DE shows consistent and slightly more pronounced benefits (Fig. 4b). These findings show that on-site PV and storage can materially compress LCOC, with direct implications for CPO cost exposure and end-user charging affordability under competitive market conditions. Sensitivity analysis using the worst- and best-case tariffs (Supplementary Figs. 8 and 9) yields results consistent with the main findings. We further test the sensitivity of our findings to time-of-use (ToU) pricing using 106 charging locations in Sweden (Supplementary Figs. 10 and 11). ToU pricing has a negligible effect on the PV-and-storage LCOC reductions, confirming the robustness of our main findings.

To examine spatial disparity, Fig. 4c summarises country-level median LCOC reductions under the average Pool-SE tariff and 373 EUR kWh^{-1} storage cost (details in Supplementary Table 2). Median reductions range 0–8% under the conservative scenario, rising to 1–16% (moderate) and 2–23% (optimistic) as deployment area expands. Country-level variation is pronounced: optimistic-scenario LCOC reductions reach 19% in Italy, 14% in Spain, and 12% in France, versus 7% in Sweden and 3% in Norway. Spatial heterogeneity persists at the station level (Fig. 4d), reflecting site-specific differences in solar resource, demand profiles, infrastructure costs, and electricity prices, and underscoring that PV and storage benefits are geographically uneven across Europe.

We further assess investment economics through station-level annualised cost savings (ACS) and payback periods (Fig. 5). Under Pool-SE (Fig. 5a), PV alone yields median ACS of 19,540 EUR, 101,402 EUR, and 166,126 EUR under the three PV-siting scenarios, respectively. Adding 373 EUR kWh^{-1} storage raises median ACS to 23,042 EUR, 124,180 EUR, and 192,367 EUR, indicating savings predominantly driven by PV with storage providing incremental gains. 100 EUR kWh^{-1} storage amplifies median ACS substantially, to 33,689 EUR, 158,919 EUR, and 257,792 EUR. Fig. 5b shows a consistent pattern in Pool-DE, with even larger increases in median ACS across the three PV-siting scenarios.

To assess whether the cost savings from solar PV and storage are sufficient to recover their upfront investment within a practical time frame, we further examine their payback periods. Under Pool-SE (Fig. 5c), payback periods are similar between PV alone and PV with 373 EUR kWh^{-1} storage, with medians of 5, 7, and 8 years across the three PV-siting scenarios. Reducing storage cost to 100 EUR kWh^{-1} shortens median payback by one (conservative) to two years (moderate/optimistic scenarios), shifting the distribution toward earlier cost recovery. Relative to PV alone, adding storage at 100 EUR kWh^{-1} increases the share of locations achieving payback within five years from 46% to 60% (conservative), 40% to 51% (moderate), and 32% to 42% (optimistic). Fig. 5d shows a consistent pattern for Pool-DE.

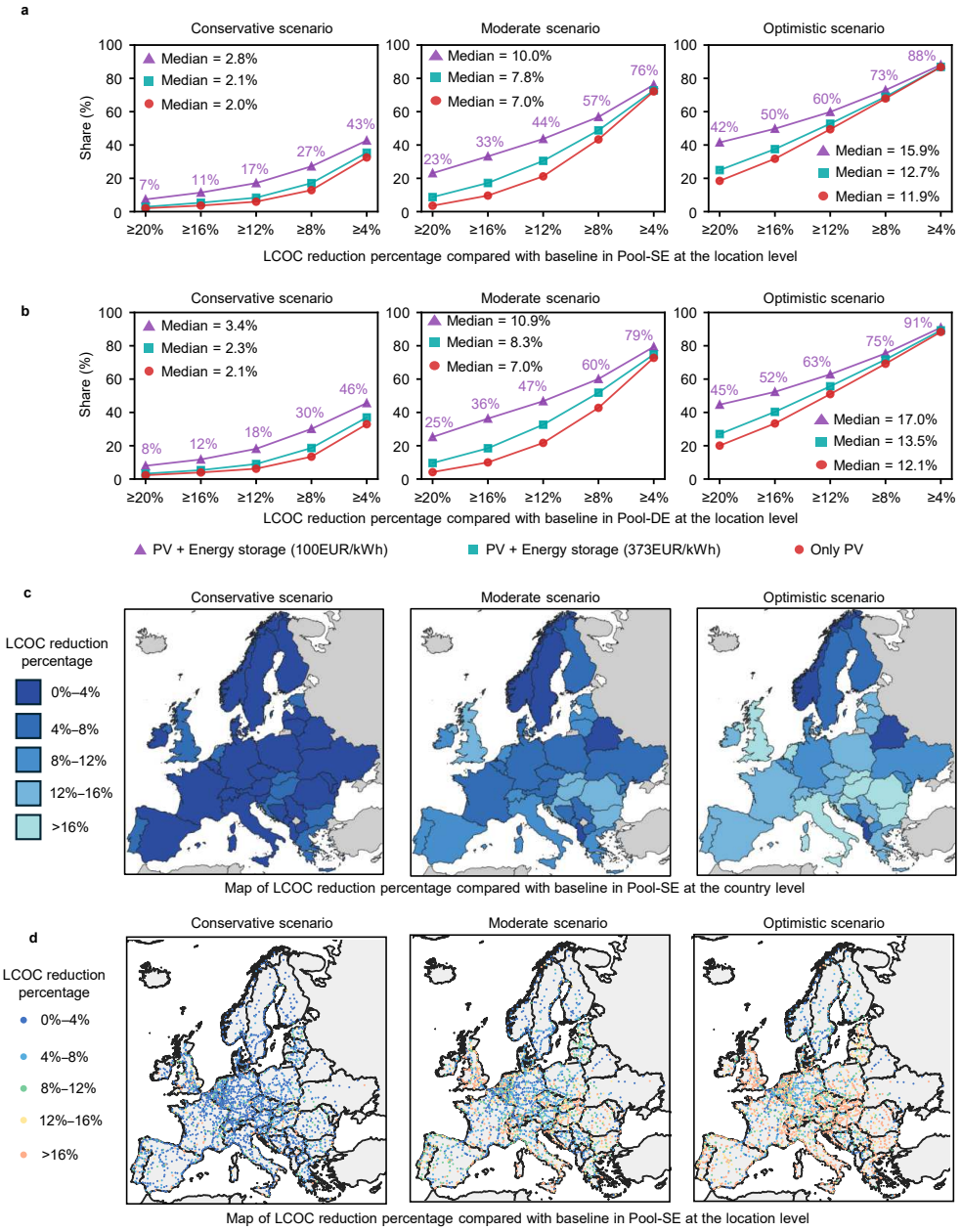

Fig. 4 **a**–**b**, Distribution of LCOC reduction percentages across charging locations under the conservative, moderate, and optimistic PV-siting scenarios, compared with the baseline in **a**, Pool-SE and **b**, Pool-DE. Storage scenarios include PV only, PV with storage at 373 EUR kWh^{-1}, and PV with storage at 100 EUR kWh^{-1}. Network tariffs are fixed at the average values in Pool-SE and Pool-DE, respectively. **c**, Country-level median percentage reduction in LCOC across charging locations under the conservative, moderate, and optimistic PV-siting scenarios, relative to the baseline. **d**, Spatial distribution of LCOC reduction percentages across charging locations under the conservative, moderate, and optimistic PV-siting scenarios, compared with the baseline. For **c**–**d**, the storage capital cost is set to 373 EUR kWh^{-1}, and the network tariff is fixed at the average value in Pool-SE.

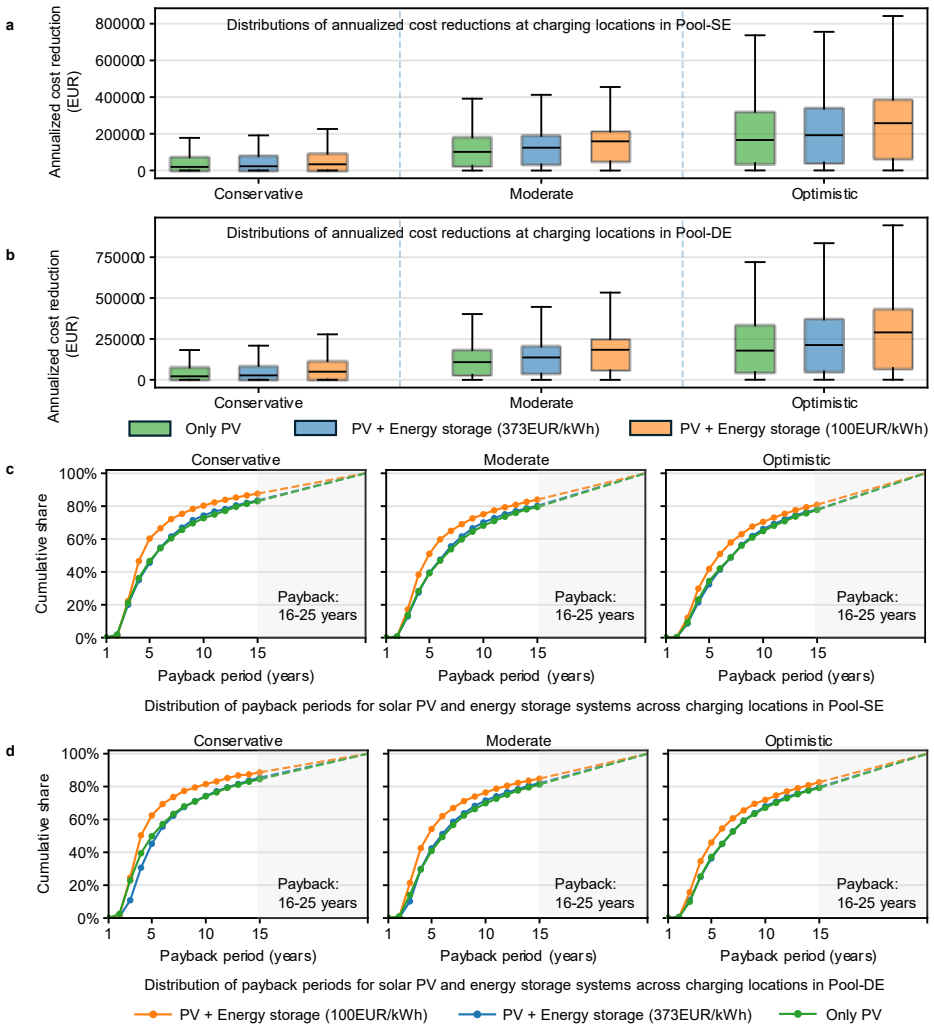

Fig. 5 **a**–**b**, Distributions of annualised cost reductions at charging locations in **a** Pool-SE and **b** Pool-DE, using average network tariff values. The annualised cost reduction is defined as the difference between the annualised baseline cost and the annualised net cost after deploying solar PV and energy storage, with the latter accounting for solar PV and energy storage costs, electricity cost savings, and feed-in tariff revenues. For each boxplot, the central line denotes the median, the box spans the 25th to 75th percentiles, and the whiskers indicate the minimum and maximum values excluding outliers. **c**–**d**, Cumulative share of discounted payback periods (in years) for solar PV and energy storage systems across charging locations in **c** Pool-SE and **d** Pool-DE, using average network tariff values. The PV-siting scenarios include conservative, moderate, and optimistic deployment assumptions. The grey shaded area denotes payback periods of 16–25 years, with dashed lines shown only for visual continuity.

Solar PV and storage compress tariff-driven LCOC difference

Beyond reducing charging costs, on-site PV and storage also mitigate the tariff-driven LCOC difference (i.e., $\Delta LCOC$) identified above. Under Pool-SE, PV alone reduces the median tariff-driven $\Delta LCOC$ from 0.042 EUR kWh^{-1} to 0.040, 0.037, and 0.035 EUR kWh^{-1} under conservative, moderate, and optimistic siting scenarios, respectively (Fig. 6a). Adding 373 EUR kWh^{-1} storage further reduces these to 0.036, 0.032, and 0.029 EUR kWh^{-1}, and 100 EUR kWh^{-1} storage compresses them to 0.032, 0.027, and 0.023 EUR kWh^{-1} under conservative, moderate, and optimistic siting scenarios, respectively. Spatial distributions of tariff-driven $\Delta LCOC$ across scenarios (Supplementary Figs. 12 and 13) reveal pronounced heterogeneity in the effectiveness of this compression: while PV and storage substantially narrow the worst-to-best tariff difference at many locations, some locations remain exposed to large worst-to-best tariff differences.

To quantify relative compression, we define a tariff-difference compression index (TDCI; Eq. (51) in Methods), measuring the fractional reduction in the worst-to-best $\Delta LCOC$ following PV-and-storage deployment (TDCI = 0: no compression; TDCI = 1: full elimination). Under Pool-SE, PV alone achieves median TDCI of 2%, 7%, and 11% across three PV-siting scenarios (Fig. 6c). Adding 373 EUR kWh^{-1} storage raises these to 5%, 17%, and 24%, while 100 EUR kWh^{-1} storage amplifies these further to 12%, 31%, and 44%, substantially shifting tariff-driven $\Delta LCOC$ distribution towards lower values. At the station level, TDCI exceeds 50% for 15%, 30%, and 45% of locations under conservative, moderate, and optimistic siting scenarios, respectively. Pool-DE results confirm consistent findings for both absolute tariff-driven $\Delta LCOC$ (Fig. 6b) and TDCI (Fig. 6d). Station-level detail (Supplementary Figs. 14 and 15) reveals pronounced spatial heterogeneity in this compression. The only-PV cases are dominated by low TDCI values, whereas the storage cases, particularly under the moderate and optimistic PV-siting scenarios, exhibit higher TDCI values on average but also greater spatial heterogeneity across locations. Overall, our results show that PV and storage substantially compress tariff-driven $\Delta LCOC$, reducing uncertainties in LCOC and investment risk across a significant share of the European charging network.

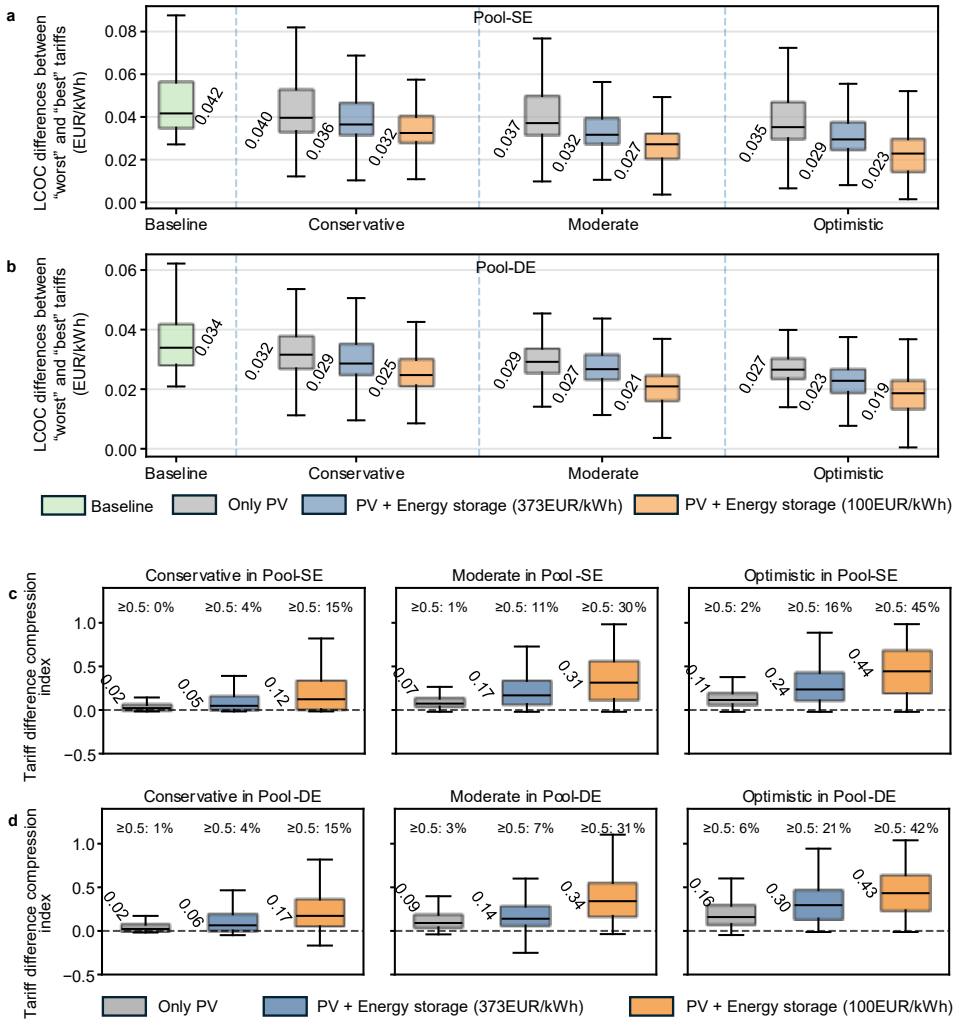

Fig. 6 **a**–**b**, Distributions of $\Delta LCOC$ between "worst" and "best" tariff scenarios across charging locations in **a**, Pool-SE and **b**, Pool-DE. For each boxplot, the central line denotes the median, the box spans the 25th to 75th percentiles, and the whiskers indicate the minimum and maximum values excluding outliers. **c**–**d**, Distributions of the tariff-difference compression index across charging locations in **c**, Pool-SE and **d**, Pool-DE. The indices are calculated using best- and worst-case DSO tariff schemes across the three PV-siting and three storage scenarios defined in Section 1.

Solar PV and storage preserve grid-connection headroom

Beyond reducing charging costs, solar PV and energy storage acting as local energy flexibility can preserve grid-connection headroom by lowering the net peak power

required from the grid. We measure this effect using the net peak-power ratio, defined as the annual maximum net grid-supplied charging power divided by installed charger capacity (see Methods). Annual maximum net grid-supplied charging power reflects the typical power grid connection power capacity requirement at a charging point in a specific year. A lower ratio in a year indicates that a charging location could operate with a smaller firm grid-connection capacity, or retain more headroom for future capacity applications as demand grows.

Figs. 7a–c show the distribution of the net peak-power ratio across charging locations over the 15-year planning horizon, using Pool-SE average network tariffs. The median ratio increases steadily over time as grid-connection capacity requirements scale with charging demand. Relative to baseline, PV alone yields only marginal reductions in a given year: an average of 0.009, 0.020 and 0.028 under the conservative, moderate and optimistic scenarios, respectively. Adding 373 EUR kWh^{-1} storage increases these to 0.053, 0.119, and 0.160. At 100 EUR kWh^{-1} storage, reductions reach 0.147, 0.255, and 0.348.

Using a net peak-power ratio of 0.5 as an illustrative threshold, the baseline median stays below this level only through year 3, and PV alone barely extends this. PV with 373 EUR kWh^{-1} storage extends it to years 4, 4, and 5 across the three scenarios, respectively. PV with 100 EUR kWh^{-1} storage extends further to years 5, 6, and 8. These results demonstrate that PV and storage can preserve grid-connection headroom by acting as local energy flexibility to offset peak charging power demand from the grid, providing CPOs with a buffer to scale grid-connection capacity gradually alongside growing charging demand. Pool-DE results (Supplementary Fig. 16) exhibit patterns consistent with the main-text findings.

Fig. 7d illustrates how storage boosts this effect by raising local PV self-consumption. Without storage, the median PV self-consumption ratios (the share of PV generation used for charging demand) are 69%, 56%, and 47% under the conservative, moderate, and optimistic PV-siting scenarios, respectively. Storage improves PV self-consumption across all scenarios: to 82%, 73%, and 59% at 373 EUR kWh^{-1} storage, and further to 92%, 87%, and 78% at 100 EUR kWh^{-1} storage. By storing excess PV generation for use in other periods, storage converts more local PV potential into usable charging energy, reducing reliance on grid electricity during peak hours and underpinning the grid-connection capacity reductions in Figs. 7a–c.

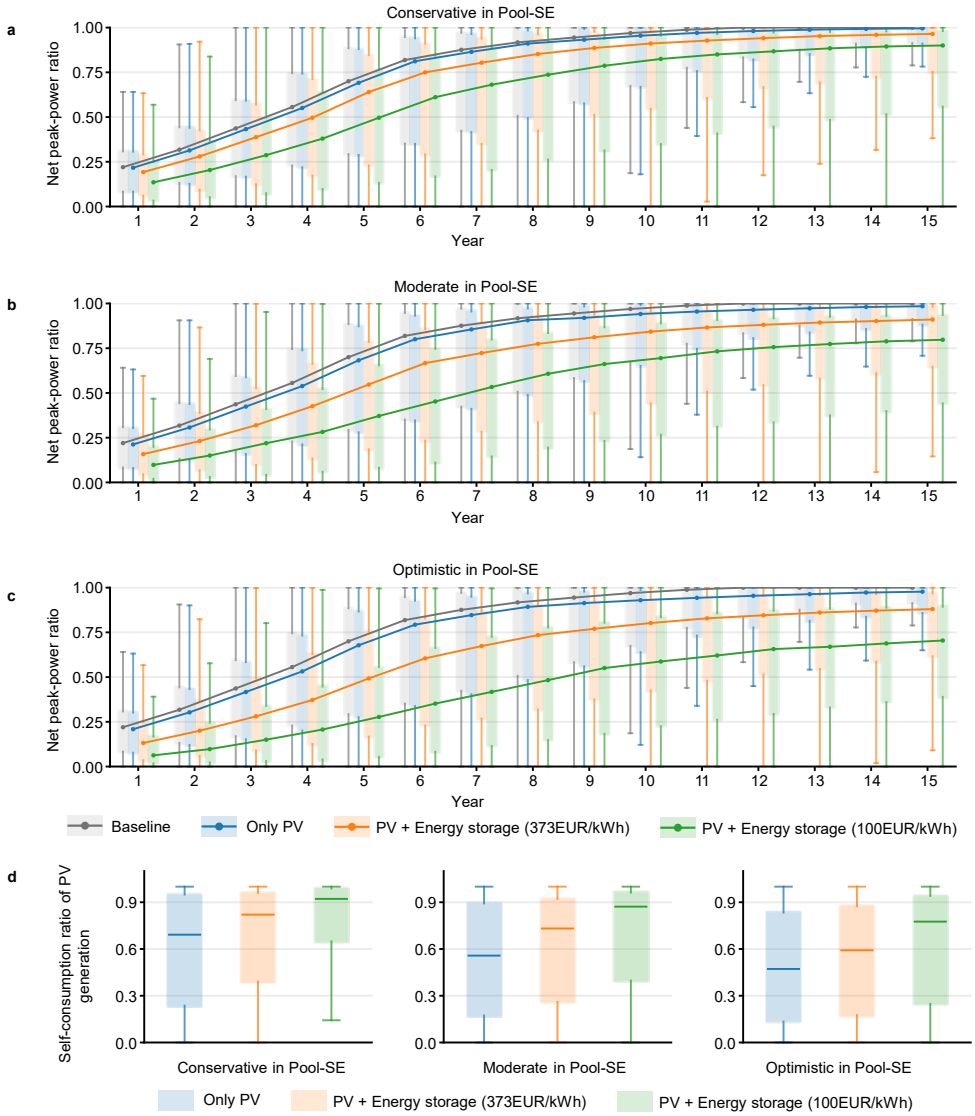

Fig. 7 **a**–**c**, Distributions of the net peak-power ratio across charging locations over the 15-year planning horizon under **a**, conservative, **b**, moderate, and **c**, optimistic PV-siting scenarios in Pool-SE. **d**, Distributions of the PV self-consumption ratio across charging locations under the three PV-siting scenarios in Pool-SE. For each boxplot, the central line denotes the median, the box spans the 25th to 75th percentiles, and the whiskers indicate the minimum and maximum values excluding outliers. Average network-tariff values are used in Pool-SE.

Discussion

Our results show that heterogeneous network tariffs strongly shape both the level and the uncertainty of long-haul truck charging costs. Solar PV and energy storage offer a dual remedy: lowering average charging costs while compressing tariff-driven cost dispersion. By reshaping net grid import, these on-site resources reduce net-load peaks and grid reliance, aligning CPO economics with grid-level benefits. Therefore, megawatt charging viability depends not only on average energy prices, but on whether charging hubs can actively manage tariff exposure and peak-power requirements. More broadly, the tariff-exposure mechanism identified here is not specific to freight charging. Any large and temporally concentrated electricity load connected to distribution grids, including fast-charging hubs, electric bus depots, electrolysers and data centres, may face substantial cost variation where network tariffs differ in their energy, power, and temporal components. Our results reveal a more general interaction between tariff design and behind-the-meter flexibility: local PV and storage can reduce not only electricity consumption costs, but also the sensitivity of operating economics to how network access is price.

The median tariff-driven $\Delta LCOC$ 0.04 EUR kWh^{-1} in Pool-SE and 0.03 EUR kWh^{-1} in Pool-DE, is comparable to the median LCOC infrastructure overhead cost, meaning network tariffs alone can tip a charging hub from commercially viable to marginal. For CPOs, this tariff exposure behaves like a location-specific capital burden that is difficult to hedge without load shaping, contract design, or regulatory clarity. A key contribution is quantifying the robustness value that on-site PV and storage provide against this heterogeneity: in Pool-SE, lowering storage costs from 373 to 100 EUR kWh^{-1} raises the share of locations where PV and storage halve tariff-driven $\Delta LCOC$ from 4–16% to 15–45% across three PV-siting scenarios. Renewable energy has been shown to deliver insurance value by stabilising electricity prices and reducing exposure to fossil-fuel price shocks [26]. Our results suggest an analogous role for site-level solar PV and storage for MCS, hedging against both average cost levels and tariff-driven dispersion as electricity-tariff structures evolve. This also suggests that exposure to network tariffs should be considered explicitly when designing and investing in emerging high-power electricity loads, rather than being treated simply as a fixed operating cost.

The net-import shaping mechanism also delivers grid-side benefits that speak directly to the connection-delay bottleneck. By lowering net peak demand, on-site PV and storage preserve grid-connection headroom as charging demand grows. In the most favourable scenario, they postpone the point at which median net peak power reaches half of grid-connection capacity from year 3 to year 8. Because this headroom is preserved within an existing grid-connection, CPOs can postpone or avoid capacity upgrades and its approval lead times, although we do not explicitly model approval timelines. Higher PV self-consumption under storage further shows that storage converts otherwise-unused local generation into usable charging energy, reducing reliance on upstream grid supply during peak periods. These effects position megawatt charging not merely as a high-power load, but as a controllable asset that can moderate its

own grid footprint as freight electrification scales, particularly relevant in power systems with heterogeneous renewable generation, network capacity, and tariff structures [27, 28].

These findings carry implications for tariff regulation and infrastructure deployment. If network tariffs are meant to reflect network cost causality, they should also give investors in high-power charging transparent and predictable signals. Otherwise, tariff-induced uncertainty risks slowing deployment even where decarbonisation benefits are high. Solar PV and storage offer one pathway to reduce this exposure, but their effectiveness hinges on siting constraints (solar irradiation, land availability), storage costs, and local tariff design. Coordinated planning between CPOs and DSOs could prioritise locations where load shaping delivers the largest combined economic and grid value, treating charging-hub siting, tariff regulation, and on-site flexibility deployment as three interdependent levers rather than separate decisions. From an energy-system perspective, this creates a feedback between tariff design, flexible-load investment, and distribution-grid capacity. Tariffs that strongly penalise coincident peaks increase the value of local flexibility, while PV and storage can in turn reshape the net-load profiles on which future network reinforcement and tariff reform are based. The freight-charging case provides a concrete demonstration of how decentralised flexibility can mediate the interaction between electrification and distribution-grid economics. This perspective broadens the relevance from charging infrastructure and transport electrification to the wider integration of new high-power loads into European distribution systems.

Several limitations apply. Pool-SE and Pool-DE capture only two tariff designs, so results indicate plausible exposure ranges rather than country-specific forecasts. PV generation uses a single weather year (2023), omitting inter-annual variability potentially shift payback and self-consumption estimates. The feed-in tariff is set equal to levelised cost, favouring larger PV systems in moderate/optimistic scenarios. Lower compensation would reduce, not eliminate storage-driven benefits. We also do not model feeder-level power flows or hosting capacity, so results reflect reductions in required connection capacity and peak import rather than avoided grid reinforcement. Future work could integrate these along with richer data or advanced driving technologies [29].

Methods

Scope. We model en-route charging demand and optimise the deployment of charging infrastructure for long-haul battery electric trucks (BETs) across the European freight network (E-network) over 2030–2044. The analysis begins in 2030 to reflect near-term (five-year) planning horizons and extends 15 years thereafter, matching the typical service lifetime of charging infrastructure (i.e., 15 years). The charging network is sited and sized to meet projected en-route charging demand in 2034, chosen as a near-term reference design year that captures the early phase of large-scale BET adoption after 2030 while avoiding the infrastructure oversizing that would result from designing directly for end-of-horizon (2044) demand. Charging demand continues to grow after 2034, and this growth is used to evaluate how utilisation, peak-load pressure, grid

tariff exposure, and the performance of on-site solar PV and storage systems evolve under a network whose siting and sizing remain fixed at the 2034 reference design. No further network expansion is modelled beyond 2034.

This study covers 36 European countries: 25 EU member states (excluding Cyprus and Malta) and 11 non-EU countries included in the European freight network (Switzerland, Norway, the United Kingdom, North Macedonia, Bosnia and Herzegovina, Serbia, Montenegro, Albania, Moldova, Ukraine, and Belarus). The analysis framework consists of four steps: (1) deriving time-resolved en-route charging demand from synthetic freight flows; (2) optimising the siting and sizing of Combined Charging System (CCS) and Megawatt Charging System (MCS) chargers; (3) assigning year-by-year charging demand to the optimised charging locations; and (4) co-optimising on-site solar PV and energy storage at each charging location. The analysis focuses on en-route charging demand; depot charging demand is outside the scope of this study.

Data. We combine five groups of input data: (1) EU freight-flow and road-network data, (2) candidate charging location data, (3) vehicle stock future projection data, (4) electricity price and network tariff data, and (5) solar resource and technology cost data. EU Freight flow and road network data are collected from the synthetic European road-freight transport flow dataset [30]. This published dataset provides estimated freight volumes in tonnes for origin–destination (OD) pairs among ETISplus NUTS-3 regions across Europe in 2010, 2019, and 2030, together with the corresponding shortest paths on the European E-network. The dataset is based on ETISplus freight OD matrices, which were calibrated against real-world traffic flows and subsequently updated using Eurostat data. Candidate charging locations are obtained from a dataset of potential European heavy-duty truck parking sites [31], which reports the coordinates and site areas of parking locations. These sites are used as candidate charging locations and are mapped to nearby E-network nodes.

Country-specific projections of heavy-duty truck stocks by powertrain type, including battery-electric trucks, are provided by the International Council on Clean Transportation (https://theicct.org/) for 2030–2044. These projections are used to scale freight flows into electric long-haul truck flows over the modelling horizon. Country-specific labour costs are compiled from multiple sources and are used to estimate charging-infrastructure capital costs, as reported in Supplementary Table 3.

Electricity-price and network-tariff data are used to evaluate electricity price in charging costs. Country-specific non-residential electricity prices are compiled from Eurostat [24] and the UK statistical data sets [25]. These prices include energy and supply costs, network costs, taxes and other charges, and are classified by electricity-consumption band. Eurostat consumption bands are used as harmonised representative average prices for consumers with comparable annual electricity consumption, rather than as marginal block tariffs. This approach provides a consistent cross-country proxy for station-level electricity procurement costs in the absence of site-specific retail contracts.

To represent heterogeneous network-tariff designs, we construct two tariff scenario pools. Pool-SE contains published 2025 tariff schemes from 115 Swedish electricity network companies, collected from the Swedish Energy Markets Inspectorate [32].

Pool-DE contains published 2026 tariff schemes from 45 German distribution system operators, collected from the respective DSO websites. To ensure comparability within each tariff pool, we only include tariffs corresponding to the same relevant customer and connection category for high-power charging applications. Tariffs from different voltage levels, customer classes, or incompatible connection categories are not mixed within the same pool. Raw tariff design data for all 160 DSOs are available in Supplementary Data 1.

We use Pool-SE and Pool-DE as tariff scenario pools rather than as geographically matched local tariffs for each charging location. Because real network-tariff data are unevenly available across Europe, the 115 Swedish and 45 German DSO schedules serve as representative test beds for tariff heterogeneity: they allow us to isolate tariff-driven cost exposure independent of country-specific energy-price levels, while avoiding inconsistent cross-country treatment of tariff components and billing determinants. A further reason is data availability, obtaining detailed local tariff data from all DSOs across the EU is impractical, if not infeasible, at the resolution required for this analysis.

The two tariff pools differ in how power-based network charges are calculated. In Pool-SE, power charges are based on monthly peak power, together with energy-based network charges. In Pool-DE, the applicable tariff category is first selected for each charging location based on its equivalent annual full-load hours, defined as annual electricity use divided by annual peak power. Following the German tariff structure, we use 2,500 h as the threshold between tariff categories and then apply the corresponding power and energy charge rates to calculate annual network costs. Pool-SE and Pool-DE therefore represent two distinct network-tariff formulations: monthly peak-power charging and annual utilisation-dependent power charging, respectively.

We use Swedish and German tariff data as representative scenario pools for the pan-European analysis for three reasons. First, Sweden and Germany exemplify two structurally distinct and widely used network tariff archetypes in Europe (demand-based charging tied to monthly peak power, and utilisation-based charging tied to annual load duration), so the two pools jointly bound a broader design space of tariff structures observed across European DSOs, rather than representing only two national cases. Second, both countries provide comprehensive and regulator-verified tariff data at DSO resolution (115 and 45 DSOs, respectively), which is not consistently available in most other European markets. This allows us to capture substantial within-country heterogeneity in tariff design, in addition to the between-country contrast captured by using two pools. Third, using tariff pools rather than location-specific national tariffs is consistent with the framework's objective: to evaluate the sensitivity of charging infrastructure economics to alternative tariff designs, rather than to produce a country-by-country cost prediction. Under this framing, exact geographic matching between charging locations and local tariffs is not required for the study's conclusions to hold.

Owing to the lack of EU-wide time-of-use (ToU) pricing data, we assume a uniform daily average energy price for each country. Because ToU pricing may affect the value of PV and storage [33, 34], we test this assumption using 106 Swedish charging locations and hourly day-ahead energy price profiles for 2023 across the four Swedish bidding zones including SE1, SE2, SE3, and SE4 [35] (Supplementary Fig. 10). For

each month, we calculate the average price for each hour of the day to construct representative hourly price profiles. These profiles are incorporated into the energy and supply component of electricity costs, while network costs, taxes, and levies are held constant and passed through to CPOs.

The effect of ToU pricing on our main findings is negligible (Supplementary Fig. 11 and detailed discussion in Supplementary Information). In most scenarios, ToU pricing marginally reduces the estimated LCOC reduction from PV and storage, with differences small enough to be considered negligible. At 100 EUR kWh^{-1} storage cost, ToU pricing yields even larger LCOC reductions. These results confirm that the country-uniform-price assumption does not overestimate the benefits of on-site PV and storage, lending further credibility to our main findings.

Grid-connection costs are excluded from the baseline LCOC because they are highly site-specific and depend on local grid conditions, reinforcement needs and DSO-specific connection rules. We instead report them separately as an indicative add-on cost, using an assumed connection fee of 150 EUR kW^{-1} [36], with country-level medians provided in Supplementary Table 1.

Solar irradiation resource and technology cost data are used to model electricity generation and capital costs of on-site PV and energy storage. Hourly meteorological variables, including 2 m air temperature, forecast albedo, and downward surface solar radiation, are obtained from the ERA5-Land monthly-averaged dataset for 2023 over European land [37]. The dataset has a horizontal resolution of approximately 9 km. Country-specific solar PV and battery-storage costs in 2030 are derived from the sources listed in Supplementary Table 4. The cost projection method is presented in Supplementary Note 2.

We define three PV-siting scenarios. In the conservative scenario, the available PV deployment area at each charging location is manually identified from Google satellite imagery (https://www.google.com/maps), including rooftop and ground areas at the mapped truck-parking site (Supplementary Data 1). In the moderate and optimistic scenarios, each charging location is assumed to have access to at least 5,000 m^2 and 10,000 m^2 of PV deployment area, respectively; where the mapped truck-parking site already provides a larger area, the larger site-specific value is retained. These moderate and optimistic areas represent achievable land allocation if charging-hub siting is co-planned with adjacent land use, rather than strictly limited to existing truck-parking footprints, and are treated as upper-bound scenarios bracketing realistic deployment. The moderate and optimistic scenarios reflect the siting flexibility allowed by the charging-infrastructure optimisation, in which candidate charging locations can lie within 10 km of an E-network node and are therefore not restricted to the mapped truck-parking site. Exported PV electricity is compensated at a feed-in tariff equal to the levelised cost of PV electricity, with no additional subsidies or marginal revenues.

Deriving time-resolved charging demand at E-network nodes. We derive time-resolved long-haul truck en-route charging demand at E-network nodes from synthetic freight flows, vehicle-stock projections, and route-level charging events. A trip between an OD pair is classified as long-haul if its total distance exceeds 350 km [38]. We focus on these long-haul OD trips, assuming that vehicles are fully charged at

departure. Depot charging is not modelled, as the analysis focuses on en-route charging demand requirements. Each OD pair is classified as a national or international trip according to the locations of its origin and destination.

We first convert freight flows in tonnes into annual loaded-truck flows in vehicles. In 2024, the average loading factors of road freight transport in the EU were 13.5 tonnes for national trips and 15.9 tonnes for international trips [39]. Given the freight flow in tonnes of an OD pair, we use the corresponding loading factor to obtain the annual loaded-truck flow in vehicles, denoted by f_{OD}^{load}. The annual flow of electric loaded long-haul trucks in 2030, $f_{OD}^{E,load}$, is then estimated as

$$f_{OD}^{E,load} = f_{OD}^{load} \frac{N_O^E + N_D^E}{N_O + N_D}, \tag{1}$$

where N_O^E and N_D^E denote the average numbers of electric heavy-duty trucks at the NUTS-3 region in the countries containing the origin and destination regions, respectively. N_O and N_D denote the corresponding average numbers of heavy-duty trucks of all powertrain types.

We also account for empty return movements using a closed-trip approximation. Eurostat reports that empty-truck vehicle-kilometres accounted for 25.8% and 12.6% of total vehicle-kilometres for national and international road-freight trips in the EU, respectively [39]. Under the assumption that each loaded OD movement is eventually associated with a return or repositioning movement over a comparable distance, these empty-VKT shares correspond to empty-return probabilities of 51.6% and 25.2% for national and international movements, respectively. For each directed loaded OD flow from origin (O) to destination (D), we therefore add an empty movement on the reverse OD direction (DO) with the corresponding empty-return probability. These empty movements are simulated separately from loaded movements, using the empty-vehicle payload state, and are assigned to the reverse shortest path on the E-network.

To represent vehicle heterogeneity, we restrict the analysis to trips whose maximum permissible laden weight exceeds 20.1 tonnes. According to Eurostat [40], 31% of these trips have a maximum permissible laden weight not exceeding 30 tonnes, while the remaining trips have a maximum permissible laden weight above 30 tonnes. We therefore assume two truck types with empty vehicle masses, excluding the battery, of 8 tonnes and 11 tonnes, assigned to 31% and 69% of trips, respectively. Battery capacities are assigned according to OD trip distance, with capacities of 600, 700, 800, 900 and 1000 kWh. The corresponding battery masses are reported in Supplementary Table 5. Combining payload, battery capacity and vehicle mass yields 30 trip types, defined by three payload states (0, 13.5 for national trips and 15.9 tonnes for international trips), five battery capacities and two empty vehicle masses.

The trip-level energy consumption rate, E, is calculated from vehicle weight following [41]:

$$E = 0.2123 \times W^{0.6672} \times F^{tech}, \tag{2}$$

where W is the total vehicle weight in tonnes and F^{tech} represents future improvements in vehicle energy efficiency. The values of F^{tech} for different battery-capacity configurations are listed in Supplementary Table 5. Eq. (2) is based on electric truck

energy consumption under current technology conditions [41], with F^{tech} introduced to account for future efficiency improvements. The energy consumption rates of 30 trip types are presented in Supplementary Table 6.

We then assign truck trips to their shortest paths on the E-network and simulate charging events along these paths. We assume one driver if the total driving time is less than 54 h and two drivers otherwise. A simplified break-and-rest rule is used to identify stopping events at E-network nodes [19]. Drivers take a 45-min break after every 4.5 h of driving and a 9-h rest after 9 h of driving. For two-driver operations, the truck stops for a 9-h rest after 18 h of driving. To increase flexibility in route-level charging, we split the 45-min break into a 15-min break after 2 h of driving and a 30-min break after another 2.5 h of driving. This split-break setting is consistent with EU driving-time rules [42]. Trucks are assumed to travel at 80 km h^{-1} along the shortest path on the E-network [43]. For detours associated with charging and break stops, the travel speed is set to 60 km h^{-1}. Each stop is assigned to the nearest E-network node along the shortest path before the required break or rest time is reached.

Charging power is set to 1000 kW during short breaks, corresponding to MCS charging, and to 100 kW during long rests, corresponding to CCS charging. The charging energy for each stopping event is calculated as:

$$Charging_demand = \begin{cases} \min\{1000 \times (Break_time - 1/12), \\ \quad (1 - SoC) \times Capacity\}, & \text{if Break,} \\ \min\{100 \times (Rest_time - 1/12), \\ \quad (1 - SoC) \times Capacity\}, & \text{if Rest.} \end{cases} \tag{3}$$

Here, $Break_time$ and $Rest_time$ are measured in hours. The term 1/12 represents a 5-min preparation time before charging. SoC denotes the battery state of charge at the start of the charging event, and $Capacity$ denotes the battery capacity.

Starting from a full battery at departure, SoC is updated sequentially along each OD route. As the truck travels between two consecutive stopping nodes, SoC decreases according to the route distance, the trip-type-specific energy consumption rate, and the battery capacity. The stopping nodes are determined by the break-and-rest rules described above. At each stopping node, charging demand is calculated using Eq. (3). After charging, SoC is updated by adding the delivered charging energy, and the truck continues to the next stopping node.

Daily truck flows are obtained by dividing annual flows by 365 days. Departure times are sampled from the discrete probability distribution derived from the DT-CARGO dataset [44], shown in Supplementary Fig. 17. Aggregating the simulated charging events by E-network node and hour gives the hourly charging demand in 2030 ($Charging_demand_{OD,node,2030}$). For subsequent years from 2031 to 2044, hourly charging demand associated with each OD pair and E-network node is scaled according

to country-level battery-electric truck stock projections:

$$Charging_demand_{OD,node,y} = \frac{N^E_{O,y} + N^E_{D,y}}{N^E_{O,2030} + N^E_{D,2030}} \times Charging_demand_{OD,node,2030}, \tag{4}$$

where $N^E_{O,y}$ and $N^E_{D,y}$ denote the average numbers of electric heavy-duty trucks per NUTS-3 region in the countries containing the origin and destination regions in year y, respectively.

Optimising deployment of long-haul truck charging infrastructure along the E-network. We first identify candidate long-haul truck charging locations by mapping potential European heavy-duty truck parking locations to nearby E-network nodes. A parking location is considered a candidate charging location for an E-network node if its Euclidean distance to that node is no greater than 10 km. This mapping provides both the set of feasible charging locations and the available site area around each E-network node, allowing us to account for additional land-expansion costs when the existing area is insufficient for charger deployment.

The study region is divided into square zones with a side length of 100 km. Charging infrastructure optimisation is solved in a zone-by-zone manner. Cross-zone flows and boundary charging demands are propagated through the network and assigned to the corresponding zones, while the resulting optimisation problem is solved separately for each zone. For each node on the E-network, charging demand may be assigned to candidate charging locations associated with the current node or with the two preceding nodes along the route, provided that the driving distance from the current node to the two preceding nodes does not exceed 50 km. Charging demand at nodes within a given zone could be served by feasible candidate charging locations in neighbouring zones. Thus, the zone is used solely to decompose the optimisation problem for tractability and does not impose hard spatial boundaries on demand–node–location assignment. The lifetime of both CCS and MCS chargers is assumed to be 15 years [45].

For each zone, we formulate a mixed-integer linear programming (MILP) model that minimises the discounted lifetime overhead cost of charging infrastructure, excluding electricity costs. The overhead cost includes charger capital costs, fixed operation and maintenance costs, land-expansion costs, and a small penalty for building additional charging locations. This penalty is set to $\epsilon = 1$ EUR per built charging location and is used only as a tie-breaker to favour solutions with fewer charging locations when infrastructure costs are otherwise identical or nearly identical. Other parameters are reported in Supplementary Table 7. Country-specific installation costs are adjusted using country-specific labour costs, as described in Supplementary Note 3.

For each zone, let I denote the set of candidate charging locations, J the set of E-network nodes, K the set of OD pairs whose shortest paths pass through nodes in J, T the set of hours in a day, and Y the set of years (1,2,...,15) in the study horizon.

The charging-infrastructure optimisation problem is formulated as

$$\min \sum_{i \in I} \Bigg[C^{CCS}_{i,capital} N^{CCS}_i + \sum_{y \in Y} \frac{C^{CCS}_{i,capital} N^{CCS}_i \times 1\%}{(1+9.5\%)^y} + C^{MCS}_{i,capital} N^{MCS}_i + \sum_{y \in Y} \frac{C^{MCS}_{i,capital} N^{MCS}_i \times 1.5\%}{(1+9.5\%)^y} + C_{expand} S_i + \epsilon x_i \Bigg]. \tag{5}$$

Here, $C^{CCS}_{i,capital}$ and $C^{MCS}_{i,capital}$ denote the capital costs of CCS and MCS chargers at candidate charging location i, respectively. N^{CCS}_i and N^{MCS}_i are the numbers of CCS and MCS chargers deployed at candidate charging location i. The second and fourth terms represent the discounted fixed operation and maintenance costs, assumed to be 1% and 1.5% of the capital costs of CCS and MCS chargers, respectively. The term $C_{expand} S_i$ represents the land-expansion cost, where C_{expand} is the expansion cost per square meter and S_i is the additional area required. The binary variable x_i equals 1 if candidate charging location i is built and 0 otherwise.

The first group of constraints determines the number of chargers required and the additional expanded area

$$N^{CCS}_i \geq \frac{d^{CCS}_{2034,i,t}}{100 \times 1}, \qquad \forall i \in I, t \in T, \tag{6}$$

$$N^{MCS}_i \geq \frac{d^{MCS}_{2034,i,t}}{1000 \times 1}, \qquad \forall i \in I, t \in T, \tag{7}$$

$$S_i \geq A \times (N^{CCS}_i + N^{MCS}_i - \bar{N}_i), \qquad \forall i \in I, \tag{8}$$

$$M x_i \geq N^{CCS}_i + N^{MCS}_i, \qquad \forall i \in I. \tag{9}$$

Here, $d^{CCS}_{2034,i,t}$ and $d^{MCS}_{2034,i,t}$ denote the CCS and MCS charging demand assigned to charging location i in hour t in 2034. A is the required area for installation and parking per charger, $\bar{N}_i$ is the maximum number of chargers that can be deployed without land expansion at candidate charging location i, and M is a sufficiently large constant.

The second group of constraints allocates hourly charging demand from OD-pair movements at E-network nodes to feasible charging locations

$$\sum_{i \in I} d^{CCS}_{2034,j,k,i,t} = D^{CCS}_{2034,j,k,t}, \qquad \forall j \in J, k \in K, t \in T, \tag{10}$$

$$\sum_{i \in I} d^{MCS}_{2034,j,k,i,t} = D^{MCS}_{2034,j,k,t}, \qquad \forall j \in J, k \in K, t \in T, \tag{11}$$

$$d^{CCS}_{2034,j,k,i,t} \leq \delta_{j,k,i} D^{CCS}_{2034,j,k,t}, \qquad \forall j \in J, k \in K, i \in I, t \in T, \tag{12}$$

$$d^{MCS}_{2034,j,k,i,t} \leq \delta_{j,k,i} D^{MCS}_{2034,j,k,t}, \qquad \forall j \in J, k \in K, i \in I, t \in T, \tag{13}$$

$$d^{CCS}_{2034,i,t} = \sum_{j \in J, k \in K} d^{CCS}_{2034,j,k,i,t}, \qquad \forall i \in I, t \in T, \tag{14}$$

$$d^{MCS}_{2034,i,t} = \sum_{j\in J, k\in K} d^{MCS}_{2034,j,k,i,t}, \qquad \forall i \in I, t \in T. \tag{15}$$

$D^{CCS}_{2034,j,k,t}$ and $D^{MCS}_{2034,j,k,t}$ are the CCS and MCS charging demands of OD pair k at E-network node j in hour t in 2034. The variables $d^{CCS}_{2034,j,k,i,t}$ and $d^{MCS}_{2034,j,k,i,t}$ represent the part of this demand assigned to candidate charging location i. The parameter $\delta_{j,k,i}$ equals 1 if the charging demand of OD pair k at E-network node j can be assigned to charging location i, and 0 otherwise. All decision variables are non-negative, and the MILP models are solved using Gurobi in Python.

Year-by-year assignment of charging demand to optimised charging locations. After the charging locations and charger capacities are determined, we assign charging demand to the optimised charging locations for each year from 2030 to 2044. This optimisation step uses the optimised infrastructure results and determines the served hourly charging demand at each location. The objective is to maximise served charging demand while minimising charging costs. This step generates the year-by-year charging profiles used in the LCOC calculation and in the subsequent on-site PV and battery-storage optimisation.

Electricity prices are represented using declining consumption bands, in which the unit electricity price decreases as annual electricity consumption moves into higher bands. Let B denote the set of electricity-consumption bands. The demand-assignment problem is formulated as

$$\min \sum_{y\in Y, i\in I, b\in B} C^{electricity}_{y,i,b} \frac{D_{y,i,b}}{(1+9.5\%)^y} - \sum_{y\in Y, i\in I} C' \frac{D_{y,i}}{(1+9.5\%)^y}. \tag{16}$$

Here, $C^{electricity}_{y,i,b}$ is the electricity price in consumption band b at charging location i in year y. $D_{y,i,b}$ denotes the served annual charging demand assigned to band b, and $D_{y,i}$ denotes the total served annual charging demand at charging location i in year y. The parameter C' is a sufficiently large weight used to prioritise served charging demand over cost minimisation, chosen to be larger than $\max\{C^{electricity}_{y,i,b} | i \in I, b \in B\}$.

The first group of constraints follows Equations (10)–(15), but is applied to each year in the study horizon. The second group of constraints links annual served demand to the corresponding electricity-consumption band:

$$D_{y,i} = 365 \sum_{t\in T} (D^{CCS}_{y,i,t} + D^{MCS}_{y,i,t}), \qquad \forall y \in Y, i \in I, \tag{17}$$

$$L_{i,b} - M(1 - z_{y,i,b}) \le D_{y,i} \le U_{i,b} + M(1 - z_{y,i,b}), \qquad \forall y \in Y, i \in I, b \in B, \tag{18}$$

$$\sum_{b\in B} z_{y,i,b} = 1, \qquad \forall y \in Y, i \in I, \tag{19}$$

$$D_{y,i} - M(1 - z_{y,i,b}) \le D_{y,i,b} \le D_{y,i} + M(1 - z_{y,i,b}), \qquad \forall y \in Y, i \in I, b \in B, \tag{20}$$

$$D_{y,i,b} \le M z_{y,i,b}, \qquad \forall y \in Y, i \in I, b \in B. \tag{21}$$

$D^{CCS}_{y,i,t}$ and $D^{MCS}_{y,i,t}$ are the served CCS and MCS charging demands at charging location i in hour t of year y. $L_{i,b}$ and $U_{i,b}$ are the lower and upper bounds of electricity-consumption band b, and the binary variable $z_{y,i,b}$ equals 1 if $D_{y,i}$ falls within band b.

The third group of constraints ensures that served demand does not exceed either the assigned charging demand or the installed charger capacity:

$$D^{CCS}_{y,i,t} \leq d^{CCS}_{y,i,t}, \qquad \forall y \in Y, i \in I, t \in T, \tag{22}$$

$$D^{CCS}_{y,i,t} \leq 100 \times 1 \times N^{CCS}_{i}, \qquad \forall y \in Y, i \in I, t \in T, \tag{23}$$

$$D^{MCS}_{y,i,t} \leq d^{MCS}_{y,i,t}, \qquad \forall y \in Y, i \in I, t \in T, \tag{24}$$

$$D^{MCS}_{y,i,t} \leq 1000 \times 1 \times N^{MCS}_{i}, \qquad \forall y \in Y, i \in I, t \in T. \tag{25}$$

All decision variables are non-negative, and the optimisation models are solved using Gurobi in Python.

Optimising capacities of solar PV and energy storage at charging locations. For each optimised charging location, we optimise the installed capacities of on-site solar PV and energy storage using the year-by-year served charging profiles obtained from the demand-assignment model. The optimisation minimises an equivalent annual cost that combines annualised PV and storage investment costs with the annualised present value of net electricity costs over the 2030–2044 study horizon. We present the formulation using Pool-SE as an example. The Pool-DE formulation differs in the calculation of network costs because the applicable German tariff category depends on annual full-load hours. This formulation is provided in Supplementary Note 4.

We first estimate the hourly output of a reference PV module at each charging location. The SunPower SPR-E20-327 module is used as the reference module [46], with module parameters reported in Supplementary Table 8. The tilt angle of the PV panels is set equal to the latitude of each charging location, and the azimuth angle is set to zero [47]. We use the PVlib Python toolbox to calculate hourly PV output profiles [48]. The 2023 profiles are used for 2030–2044, with year-by-year PV degradation applied to the module output. Energy storage is modelled as a one-hour system with a fixed 1C power rating.

Let Y, H, T and O denote the sets of years, months, hours in a day and intra-hour sub-periods, respectively. The set O represents intra-hour load segments, allowing charging events with fractional-hour durations to be represented in the PV-storage optimisation. Let Δ_o denote the duration of sub-period o. The served CCS and MCS charging demand profiles are converted into an intra-hour charging-load profile, denoted by $L_{y,t,o}$, before the PV-storage optimisation. This load profile is treated as an exogenous input to the PV-storage model.

The capacity decision variables are the installed PV capacity, P^{PV}, and the installed battery-storage energy capacity, E^{B}. The model also tracks four electricity flows. Let $S^{PV,E}_{y,h,t,o}$ denote PV electricity directly used for truck charging, $S^{B,E}_{y,h,t,o}$ denote battery discharge used for truck charging, $S^{PV,B}_{y,h,t,o}$ denote PV electricity stored in the

battery, and $S^{G,B}_{y,h,t,o}$ denote grid electricity used to charge the battery. A separate variable for exported PV electricity is not introduced, as it is a redundant variable that can be expressed as the residual PV generation after direct truck charging and battery charging. The remaining battery energy after hour t is denoted by $E^{B}_{y,h,t}$.

The discount rate is set to $r = 9.5\%$. For a technology with lifetime n, the capital recovery factor is

$$CRF(n) = \frac{r(1+r)^n}{(1+r)^n - 1}. \tag{26}$$

The lifetimes of PV, energy storage and charging infrastructure are set to 25, 15 and 15 years, respectively. We therefore define $CRF_{PV} = CRF(25)$, $CRF_B = CRF(15)$ and $CRF_{CI} = CRF(15)$. Let c^{PV}_{cap} and c^{PV}_{om} denote the unit capital and O&M costs of PV, and let c^{B}_{cap} and c^{B}_{om} denote the corresponding costs of energy storage. The O&M cost of storage includes the cost of replenishing capacity to compensate for battery degradation. Accordingly, the installed storage capacity is assumed to remain unchanged over the planning horizon, without explicit year-by-year capacity decay. The feed-in tariff for exported PV electricity, FiT, is set equal to the levelised cost of PV electricity at the corresponding charging location.

The objective function minimises the equivalent annual cost

$$\begin{aligned} \min \quad & (c^{PV}_{cap} CRF_{PV} + c^{PV}_{om}) P^{PV} \\ & + (c^{B}_{cap} CRF_{B} + c^{B}_{om}) E^{B} \\ & + CRF_{CI} \sum_{y \in Y} \frac{NC^{SE}_{y}}{(1+r)^y}. \end{aligned} \tag{27}$$

The first two terms represent the annualised investment and O&M costs of PV and energy storage. The third term converts the discounted net electricity costs over the charging-infrastructure lifetime into an equivalent annual cost using CRF_{CI}. NC^{SE}_{y} denotes the annual net electricity cost under the Pool-SE tariff formulation.

PV deployment is constrained by the available area at each charging location. Let P^{mod} and A^{mod} denote the rated power and area of the reference PV module, respectively. Let A^{ava}_{i} denote the available PV deployment area at charging location i, and let θ_i denote the PV tilt angle. We assume that inter-panel spacing occupies 20% of the available area. The PV area constraint is

$$\frac{P^{PV}}{P^{mod}} A^{mod} \cos(\theta_i) \leq 0.8 A^{ava}_{i}. \tag{28}$$

Our PV generation estimation accounts for inverter efficiency and the area-based packing constraint, but does not explicitly model additional balance-of-system losses, such as shading, wiring losses, or other site-specific effects. This simplification is partly offset by the conservative reference module used in the analysis. The selected SunPower SPR-E20-327 module has an efficiency of 20.1%, which is lower than recent high-efficiency commercial modules and expected future technology improvements, with reported module efficiencies of around 22.7% or higher [49]. We therefore interpret the

PV output estimates as a conservative representation of future on-site PV potential, while acknowledging that actual site-level losses may vary across charging locations.

The electricity supplied by PV and storage to trucks cannot exceed the charging load

$$S^{PV,E}_{y,h,t,o} + S^{B,E}_{y,h,t,o} \leq L_{y,t,o}\Delta_o, \quad \forall y,h,t,o. \tag{29}$$

The use of PV electricity is limited by the available PV generation:

$$S^{PV,E}_{y,h,t,o} + S^{PV,B}_{y,h,t,o} \leq \frac{P^{PV}}{P^{mod}} p^{PV}_{y,h,t}\Delta_o, \quad \forall y,h,t,o, \tag{30}$$

where $p^{PV}_{y,h,t}$ denotes the hourly output of one reference PV module in year y, month h and hour t, including PV degradation.
Storage charging and discharging power are constrained by a C-rate of one [50]

$$S^{B,E}_{y,h,t,o} \leq E^B\Delta_o, \qquad \forall y,h,t,o, \tag{31}$$

$$S^{PV,B}_{y,h,t,o} + S^{G,B}_{y,h,t,o} \leq E^B\Delta_o, \qquad \forall y,h,t,o. \tag{32}$$

The battery energy balance is

$$\begin{aligned} E^B_{y,h,t} = E^B_{y,h,t-1} &- \sum_{o\in O} S^{B,E}_{y,h,t,o} \\ &+ \sum_{o\in O} S^{PV,B}_{y,h,t,o} + \sum_{o\in O} S^{G,B}_{y,h,t,o}, \quad \forall y,h,t. \end{aligned} \tag{33}$$

The battery state of charge is bounded between 10% and 100% of installed storage capacity:

$$0.1E^B \leq E^B_{y,h,t} \leq E^B, \quad \forall y,h,t. \tag{34}$$

For the representative day of each month, the battery energy level at the beginning and end of the day is constrained to be identical:

$$E^B_{y,h,0} = E^B_{y,h,|T|}, \quad \forall y,h. \tag{35}$$

This cyclic boundary condition reflects the use of a representative-day formulation, in which day-to-day storage dynamics are not explicitly modelled. It ensures that storage operation within each representative day is energy-neutral.

To avoid simultaneous charging and discharging within the same hour, we introduce a binary variable $w^B_{y,h,t}$, which equals 1 when the battery discharges to serve truck charging and 0 otherwise:

$$\sum_{o\in O} S^{B,E}_{y,h,t,o} \leq M w^B_{y,h,t}, \qquad \forall y,h,t, \tag{36}$$

$$\sum_{o\in O} \left(S^{PV,B}_{y,h,t,o} + S^{G,B}_{y,h,t,o}\right) \leq M(1 - w^B_{y,h,t}), \qquad \forall y,h,t, \tag{37}$$

where M is a sufficiently large constant.

Under the Pool-SE formulation, the annual net electricity cost consists of non-network electricity costs, network energy charges, monthly peak-power charges and revenue from exported PV electricity:

$$\begin{aligned} NC_y^{SE} = (c_y^{oth} + c^{SE,en})G_y \\ + c^{SE,pw} \sum_{h \in H} P_{y,h}^{peak} \\ - FiTX_y, \quad \forall y. \end{aligned} \tag{38}$$

Here, c_y^{oth} is the electricity price component excluding network charges, determined from the country-specific non-residential electricity price and the corresponding electricity-consumption band in year y. $c^{SE,en}$ and $c^{SE,pw}$ are the energy-based network charge and monthly peak-power charge under the selected Pool-SE tariff scenario, respectively.

Annual grid-supplied charging demand is calculated as:

$$\begin{aligned} G_y = 365 \sum_{t \in T} \sum_{o \in O} L_{y,t,o} \Delta_o \\ - \sum_{h \in H} \sum_{t \in T} \sum_{o \in O} D_h \left(S_{y,h,t,o}^{PV,E} + S_{y,h,t,o}^{B,E} \right) \\ + \sum_{h \in H} \sum_{t \in T} \sum_{o \in O} D_h S_{y,h,t,o}^{G,B}, \quad \forall y, \end{aligned} \tag{39}$$

where D_h is the number of days in month h. This definition counts grid electricity used to charge the battery as part of grid-supplied demand.

Exported PV electricity is calculated as:

$$\begin{aligned} X_y = \sum_{h \in H} \sum_{t \in T} D_h \frac{P^{PV}}{P^{mod}} p_{y,h,t}^{PV} \\ - \sum_{h \in H} \sum_{t \in T} \sum_{o \in O} D_h \left(S_{y,h,t,o}^{PV,E} + S_{y,h,t,o}^{PV,B} \right), \quad \forall y. \end{aligned} \tag{40}$$

Monthly peak power at the hour level is determined from the maximum net grid-supplied load in each month:

$$\begin{aligned} P_{y,h}^{peak} \times 1 \geq \sum_{o \in O} L_{y,t,o} \Delta_o - \sum_{o \in O} S_{y,h,t,o}^{PV,E} \\ - \sum_{o \in O} S_{y,h,t,o}^{B,E} + \sum_{o \in O} S_{y,h,t,o}^{G,B}, \quad \forall y, h, t. \end{aligned} \tag{41}$$

This definition ensures that both direct grid supply to truck charging and grid electricity used to charge the battery contribute to the monthly peak-power charge. All decision variables are non-negative, and the MILP models are solved using Gurobi in

Python. Supplementary Tables 9 and 10 summarise the temporal structure of the optimisation model and report the number of optimisation instances solved across tariff pools, tariff settings, PV siting assumptions, and storage-cost scenarios.

Economic performance metrics. For each charging location, we calculate the LCOC as the ratio between equivalent annual cost and equivalent annual served charging demand over the 15-year charging-infrastructure lifetime. Let $r = 9.5\%$ denote the discount rate, Y the set of years in the study horizon, and CRF_{CI} the capital recovery factor for the 15-year charging-infrastructure lifetime. Let $Q_{i,y}$ denote the served charging demand at charging location i in year y. The equivalent annual served charging demand is:

$$\bar{Q}_i = CRF_{CI} \sum_{y \in Y} \frac{Q_{i,y}}{(1+r)^y}. \tag{42}$$

For the baseline case without on-site solar PV and energy storage, the equivalent annual cost is:

$$\begin{aligned} \overline{C}_i^{base} = {} & CRF_{CI} \left(C_i^{CI,cap} + C_i^{land} \right) \\ & + CRF_{CI} \sum_{y \in Y} \frac{C_{i,y}^{CI,om} + C_{i,y}^{grid,base}}{(1+r)^y}, \end{aligned} \tag{43}$$

where $C_i^{CI,cap}$ is the charging-infrastructure capital cost, C_i^{land} is the parking-area expansion cost, $C_{i,y}^{CI,om}$ is the charging-infrastructure O&M cost, and $C_{i,y}^{grid,base}$ is the annual electricity cost paid to the grid in the baseline case. The baseline LCOC is:

$$LCOC_i^{base} = \frac{\overline{C}_i^{base}}{\bar{Q}_i}. \tag{44}$$

For scenarios with on-site solar PV and energy storage, the equivalent annual cost is:

$$\begin{aligned} \overline{C}_i^{DER} = {} & CRF_{CI} \left(C_i^{CI,cap} + C_i^{land} \right) \\ & + CRF_{CI} \sum_{y \in Y} \frac{C_{i,y}^{CI,om} + NC_{i,y}}{(1+r)^y} \\ & + \left(c_{cap}^{PV} CRF_{PV} + c_{om}^{PV} \right) P_i^{PV} \\ & + \left(c_{cap}^{B} CRF_{B} + c_{om}^{B} \right) E_i^{B}. \end{aligned} \tag{45}$$

Here, $NC_{i,y}$ is the annual net electricity cost after deploying on-site PV and energy storage, including grid electricity costs, network charges and revenue from exported PV electricity. P_i^{PV} and E_i^B are the optimised PV and battery-storage capacities. c_{cap}^{PV} and c_{om}^{PV} are the unit capital and O&M costs of PV, while c_{cap}^{B} and c_{om}^{B} are the corresponding costs of energy storage. The LCOC with on-site energy resources is:

$$LCOC_i^{DER} = \frac{\overline{C}_i^{DER}}{\bar{Q}_i}. \tag{46}$$

The percentage reduction in LCOC is calculated as:

$$R_i^{LCOC} = \frac{LCOC_i^{base} - LCOC_i^{DER}}{LCOC_i^{base}} \times 100\%. \tag{47}$$

We also calculate the equivalent annual cost saving:

$$S_i^{ann} = \overline{C}_i^{base} - \overline{C}_i^{DER}. \tag{48}$$

The payback period is defined as the first integer year in which cumulative discounted electricity-cost savings recover the upfront PV and battery-storage investment. Let I_i^{DER} denote the upfront investment in on-site PV and energy storage:

$$I_i^{DER} = c_{cap}^{PV} P_i^{PV} + c_{cap}^{B} E_i^{B}. \tag{49}$$

The discounted payback period is:

$$Payback_i = \min \left\{ \tau \in \{1, \ldots, |Y|\} : \sum_{y=1}^{\tau} \frac{C_{i,y}^{grid,base} - NC_{i,y}}{(1+r)^y} \geq I_i^{DER} \right\}. \tag{50}$$

We find that shorter paybacks are consistently associated with higher PV self-consumption: locations recovering the investment within five years typically have PV self-consumption ratios above 0.75, whereas those with paybacks exceeding 15 years generally have ratios below 0.1 (Supplementary Figs. 18 and 19). To synthesise these economic metrics, we define an economic-performance criterion requiring either a LCOC reduction of $\geq$10% or annualised savings of $\geq$100,000 EUR, subject to a payback period of no more than 10 years. Under Pool-SE at 373 EUR kWh^{-1} storage cost, 18%, 65%, and 65% of charging locations satisfy this criterion under conservative, moderate, and optimistic siting scenarios, respectively (Supplementary Fig. 20). Reducing storage costs to 100 EUR kWh^{-1} raises these shares by 13, 7, and 5 percentage points. Pool-DE results are consistent (Supplementary Fig. 20).

Tariff-difference compression index, grid-connection and solar-use metrics. For each charging location i, we define the baseline best-case and worst-case LCOC values as $LCOC_i^{base,best}$ and $LCOC_i^{base,worst}$, respectively. These correspond to the lowest and highest LCOC values across the tariff schemes in a given network-tariff pool. After deploying on-site PV and energy storage, we denote the LCOC under the baseline worst-case and best-case tariff schemes as $LCOC_i^{DER,worst}$ and $LCOC_i^{DER,best}$, respectively. The TDCI measures the fractional reduction in the tariff-driven LCOC difference:

$$TDCI_i = \frac{\left(LCOC_i^{base,worst} - LCOC_i^{base,best}\right) - \left(LCOC_i^{DER,worst} - LCOC_i^{DER,best}\right)}{LCOC_i^{base,worst} - LCOC_i^{base,best}}. \tag{51}$$

To evaluate grid-connection feasibility, we define the net peak-power ratio as:

$$NPPR_{i,y} = \frac{\max_{h,t} P^{net}_{i,y,h,t}}{100N_i^{CCS} + 1000N_i^{MCS}}, \tag{52}$$

where $P^{net}_{i,y,h,t}$ is the net grid-supplied charging power at charging location i in year y, month h and hour t. The denominator is the installed charger capacity, calculated from the numbers of CCS and MCS chargers.

The PV self-consumption ratio is defined as:

$$SCR_i = \frac{\sum_{y,h,t,o} D_h \left(S^{PV,E}_{i,y,h,t,o} + S^{PV,B}_{i,y,h,t,o} \right)}{\sum_{y,h,t} D_h \frac{P_i^{PV}}{P^{mod}} p^{PV}_{i,y,h,t}}. \tag{53}$$

This ratio measures the share of local PV generation that is either directly used for truck charging or stored in the battery for later use.

Data availability

The data that support the findings of this study are available within the article, Supplementary Information, Supplementary Data 1, Supplementary Data 2, and Supplementary Data 3.

Acknowledgments

This research was supported by research funding from the Area of Advance Transport at Chalmers University of Technology, and by the Swedish Energy Agency (Energimyndigheten, grant no. P2025-04484). Any opinions, findings, and conclusions or recommendations expressed in this paper are those of the authors and do not necessarily reflect the views of the sponsors.

The authors used AI-based tools solely to improve the English language and readability of the manuscript after all content had been written by the authors. These tools were not used for content generation, data analysis, or any other purpose, and the authors take full responsibility for the content of the publication.

Author contributions

X.L.: Conceptualisation, Methodology, Investigation, Formal analysis, Data curation, Writing – original draft, Writing – review& editing. P.P.: Investigation, Validation, Data curation, Writing – review & editing. S.Y.: Investigation, Validation, Data curation, Writing – review& editing. X.Q.: Validation, Writing – review & editing. K.G.: Conceptualisation, Methodology, Investigation, Formal analysis, Data curation, Supervision, Project administration, Funding acquisition, Writing – original draft, Writing – review & editing.

References

[1] International Energy Agency. Tracking trucks and buses (2025). https://www.iea.org/energy-system/transport/trucks-and-buses.

[2] Aryanpur, V. & Rogan, F. Decarbonising road freight transport: The role of zero-emission trucks and intangible costs. *Sci Rep* **14** (2024).

[3] Schneider, J., Teichert, O., Zähringer, M., Balke, G. & Lienkamp, M. The novel megawatt charging system standard: Impact on battery size and cell requirements for battery-electric long-haul trucks. *eTransportation* **17**, 100253 (2023).

[4] Muratori, M. *et al.* Technology solutions to mitigate electricity cost for electric vehicle DC fast charging. *Appl. Energy* **242**, 415–423 (2019).

[5] Muratori, M., Kontou, E. & Eichman, J. Electricity rates for electric vehicle direct current fast charging in the United states. *Renew. Sust. Energ. Rev.* **113**, 109235 (2019).

[6] Li, Y. & Jenn, A. Impact of electric vehicle charging demand on power distribution grid congestion. *Proc. Natl. Acad. Sci. U. S. A.* **121**, e2317599121 (2024).

[7] Borlaug, B. *et al.* Heavy-duty truck electrification and the impacts of depot charging on electricity distribution systems. *Nat. Energy* **6**, 673–682 (2021).

[8] Powell, S., Cezar, G. V., Min, L., Azevedo, I. M. L. & Rajagopal, R. Charging infrastructure access and operation to reduce the grid impacts of deep electric vehicle adoption. *Nat. Energy* **7**, 932–945 (2022).

[9] Steinbach, S. A. & Blaschke, M. J. How grid reinforcement costs differ by the income of electric vehicle users. *Nat. Commun.* **15** (2024).

[10] European Union Agency for the Cooperation of Energy Regulators. Electricity infrastructure development to support a competitive and sustainable energy system (2024). https://www.acer.europa.eu/sites/default/files/documents/Publications/ACER_2024_Monitoring_Electricity_Infrastructure.pdf.

[11] Mateo, C. *et al.* European representative electricity distribution networks. *Int. J. Electr. Power Energy Syst.* **99**, 273–280 (2018).

[12] European Union Agency for the Cooperation of Energy Regulators. Report on distribution tariff methodologies in Europe (2021). https://www.elder.org.tr/Webkontrol/uploads/Fck/caa91eed-2838-42bd-820c-b43e392ef625.pdf.

[13] European Union Agency for the Cooperation of Energy Regulators. Getting the price signals right: ACER's principles for fair and cost-reflective electricity network tariffs (2025). https://www.acer.europa.eu/news/getting-price-signals-right-fair-and-cost-reflective-electricity-network-tariffs.

[14] European Union Agency for the Cooperation of Energy Regulators. Report on electricity transmission and distribution tariff methodologies in Europe (2023). https://www.acer.europa.eu/sites/default/files/documents/Publications/ACER_electricity_network_tariff_report.pdf.

[15] Plötz, P., Sgaramella, A., Link, S., Speth, D. & Gnann, T. Future demand and costs of megawatt charging for battery electric trucks (2025). Paper presented at International Electric Vehicle Symposium & Exhibition 2025.

[16] Hoppe, J. *et al.* Cost competitiveness of alternative heavy-duty truck technologies under real-world utilisation profiles. *Nat. Commun.* **17**, 8013 (2026).

[17] Porzio, J. *et al.* Electrifying long-haul freight trucks reduces societal costs in the united states. *Nat. Commun.* **17**, 468 (2025).

[18] Speth, D., Sauter, V. & Plötz, P. Where to charge electric trucks in Europe—Modelling a charging infrastructure network. *World Electr. Vehicle J.* **13** (2022).

[19] Shoman, W., Yeh, S., Sprei, F., Plötz, P. & Speth, D. Battery electric long-haul trucks in Europe: Public charging, energy, and power requirements. *Transport. Res. Part D-Transport. Environ.* **121**, 103825 (2023).

[20] Speth, D. & Plötz, P. Depot slow charging is sufficient for most electric trucks in Germany. *Transport. Res. Part D-Transport. Environ.* **128**, 104078 (2024).

[21] Wu, T., Fainman, E., Maïzi, Y., Shu, J. & Li, Y. Allocate electric vehicles' public charging stations with charging demand uncertainty. *Transport. Res. Part D-Transport. Environ.* **130**, 104178 (2024).

[22] Sun, C., Zhao, X., Qi, B., Xiao, W. & Zhang, H. Economic and environmental analysis of coupled PV-energy storage-charging station considering location and scale. *Appl. Energy* **328**, 119680 (2022).

[23] Ozturk, Z., Demirci, A., Terkes, M. & Yumurtaci, R. Optimal planning of solar PV-based electric vehicle charging stations empowered by energy storage system: Feasibility and green charge potential. *Renew. Energy* **255**, 123715 (2025).

[24] Eurostat. Database (2025). https://ec.europa.eu/eurostat/web/main/data/database.

[25] GOV.UK. Statistical data sets (2025). https://www.gov.uk/government/statistical-data-sets.

[26] Simon, D. N. & Anadon, L. D. Power price stability and the insurance value of renewable technologies. *Nat. Energy* **10**, 329–341 (2025).

[27] López Prol, J., de Llano Paz, F., Calvo-Silvosa, A., Pfenninger, S. & Staffell, I. Wind-solar technological, spatial and temporal complementarities in Europe: A portfolio approach. *Energy* **292**, 130348 (2024).

[28] Zheng, D. *et al.* Strategies for climate-resilient global wind and solar power systems. *Nature* **643** (2025).

[29] Cheng, H. *et al.* Truck platooning reshapes greenhouse gas emissions of the integrated vehicle-road infrastructure system. *Nat. Commun.* **14**, 4495 (2023).

[30] Speth, D., Sauter, V., Plötz, P. & Signer, T. Synthetic European road freight transport flow data. *Data Brief* **40**, 107786 (2022).

[31] Link, S. & Plötz, P. Geospatial truck parking locations data for Europe. *Data Brief* **54**, 110277 (2024).

[32] Swedish Energy Markets Inspectorate. Network tariffs: Electricity network fees (2025). https://ei.se/om-oss/statistik-och-oppna-data/natavgifter---elnat.

[33] Ding, H., Hu, Z. & Song, Y. Value of the energy storage system in an electric bus fast charging station. *Applied Energy* **157**, 630–639 (2015). URL https://www.sciencedirect.com/science/article/pii/S0306261915000744.

[34] Sani Hassan, A., Cipcigan, L. & Jenkins, N. Optimal battery storage operation for PV systems with tariff incentives. *Applied Energy* **203**, 422–441 (2017). URL https://www.sciencedirect.com/science/article/pii/S030626191730778X.

[35] entsoe. Transparency platform (2026). https://transparency.entsoe.eu/.

[36] Plötz, P. *et al.* Hydrogen refuelling and charging infrastructure for trucks in Europe: A cost comparison. Preprint at https://doi.org/10.2139/ssrn.5149772 (2025).

[37] Copernicus Climate Change Service. ERA5-Land monthly averaged data from 1950 to present (2025). https://cds.climate.copernicus.eu/datasets/reanalysis-era5-land-monthly-means?tab=overview.

[38] Mareev, I., Becker, J. & Sauer, D. U. Battery dimensioning and life cycle costs analysis for a heavy-duty truck considering the requirements of long-haul transportation. *Energies* **11** (2018).

[39] Eurostat. Road freight transport by journey characteristics (2025). https://ec.europa.eu/eurostat/statistics-explained/index.php?title=Road_freight_transport_by_journey_characteristics.

[40] Eurostat. Road freight transport by maximum permissible laden weight of vehicle (2025). https://ec.europa.eu/eurostat/databrowser/view/road_go_ta_mplw/default/table?lang=en&category=road.road_go.road_go_tot.

[41] Liimatainen, H., van Vliet, O. & Aplyn, D. The potential of electric trucks – An international commodity-level analysis. *Appl. Energy* **236**, 804–814 (2019).

[42] European Commission. Driving time and rest periods (2006). https://transport.ec.europa.eu/transport-modes/road/social-provisions/driving-time-and-rest-periods_en.

[43] Bergqvist, R., Monios, J. & Jönsson, J. Potential for rapid adoption of battery-electric heavy-duty trucks for pre- and post-haulage at intermodal terminals. *Res. Transp. Bus. Manag.* **50**, 101035 (2023).

[44] Balke, G. & Adenaw, L. Heavy commercial vehicles' mobility: Dataset of trucks' anonymized recorded driving and operation (DT-CARGO). *Data Brief* **48**, 109246 (2023).

[45] Lanz, L., Noll, B., Schmidt, T. S. & Steffen, B. Comparing the levelized cost of electric vehicle charging options in Europe. *Nat. Commun.* **13** (2022).

[46] EnergySage. SunPower SPR-E20-327 solar panel (2025). https://www.energysage.com/equipment/solar-panels/sunpower/spr-e20-327-ce9611fa/.

[47] Hafez, A., Soliman, A., El-Metwally, K. & Ismail, I. Tilt and azimuth angles in solar energy applications – A review. *Renew. Sust. Energ. Rev.* **77**, 147–168 (2017).

[48] pvlib python contributors. pvlib python: Open source photovoltaic performance modeling (2025). https://pvlib-python.readthedocs.io/en/stable/.

[49] Fraunhofer Institute for Solar Energy Systems ISE. Photovoltaics report (2025). https://www.ise.fraunhofer.de/en/publications/studies/photovoltaics-report.html.

[50] Long, M., Simpkins, T., Cutler, D. & Anderson, K. A statistical analysis of the economic drivers of battery energy storage in commercial buildings (2016). In *2016 North American Power Symposium (NAPS)*, 1–6 (IEEE).

Supplementary Files

This is a list of supplementary files associated with this preprint. Click to download.

- SupplementaryData1.xlsx
- SupplementaryData2.zip
- SupplementaryData3.zip
- Supplementaryinformation.docx